Lab on a Chip

PAPER

View Article Online
View Journal | View Issue

Cite this: *Lab Chip*, 2020, **20**, 4273

Constant-potential environment for activating and synchronizing cardiomyocyte colonies with on-chip ion-depleting perm-selective membranes†

Vivek Yadav,[ab] Nicholas Chong,‡[c] Bradley Ellis,‡[c] Xiang Ren,[c] Satyajyoti Senapati,[abd] Hsueh-Chia Chang *[abcd] and Pinar Zorlutuna *[acd]

Received 10th August 2020,
Accepted 8th October 2020

DOI: 10.1039/d0lc00809e

rsc.li/loc

In this study, an ion depleted zone created by an ion-selective membrane was used to impose a high and uniform constant extracellular potential over an entire ~1000 cell rat cardiomyocyte (rCM) colony on-a-chip to trigger synchronized voltage-gated ion channel activities while preserving cell viability, thus extending single-cell voltage-clamp ion channel studies to an entire normalized colony. Image analysis indicated that rCM beating was strengthened and accelerated (by a factor of ~2) within minutes of ion depletion and the duration of contraction and relaxation phases was significantly reduced. After the initial synchronization, the entire colony responds collectively to external potential changes such that beating over the entire colony can be activated or deactivated within 0.1 s. These newly observed collective dynamic responses, due to simultaneous ion channel activation/deactivation by a uniform constant-potential extracellular environment, suggest that perm-selective membrane modules on cell culture chips can facilitate studies of extracellular cardiac cell electrical communication and how ion-channel related pathologies affect cardiac cell synchronization. The future applications of this new technology can lead to better drug screening platforms for cardiotoxicity as well as platforms that can facilitate synchronized maturation of pluripotent stem cells into colonies with high electrical connectivity.

Introduction

Exogenous electric fields, though underappreciated, find relevance for tissue engineering applications in circadian rhythm, cancer progression, wound healing, and pluripotent stem cell maturation and regeneration.[1–6] Exogenous fields have been applied to electrically excitable cells such as cardiomyocytes to biomimic the *in vivo* environment.[7] Both alternating (AC) and direct (DC) current stimulations have been shown to promote cardiomyocyte (CM) contraction in long term cultures that could otherwise show a decrease in contractile properties over time.[8–10] Additionally, various advanced microfluidic techniques have been utilized to apply electrical stimulations to heart-on-chip platforms for cardiotherapeutic drug screening studies, disease modeling, and monitoring of CM contractile properties.[11–13] The AC field is commonly used in cardiac development, defibrillation and pacing cells to a desired physiological frequency.[14] The AC field has also been used to mature pluripotent stem cells into cardiomyocytes.[6,15] Exogenous fields typically have low amplitude (1–6 V cm^{-1}) and low frequency (0.1–6 Hz), with a (0.25–10 ms) monophasic/biphasic square/sinusoidal pulse waveform.[16] A short-duration (~ms) but high power AC field has also been shown to successfully treat cardiac dysrhythmias.[17] Although the threshold for defibrillation is around 6–36 V cm^{-1}, a much higher field is required to counter the signal loss in the skin. Unfortunately, electric fields beyond 50 V cm^{-1} lead to irreversible and potentially lethal cellular damage.[18–20] Additionally, both DC and AC currents that exceed ~3 mA lead to harmful faradaic products, pH changes, and high Joule heating (~tens of mW) causing additional cell death along with undesirable air bubble formation in microchannels.[7,19–21] Also, a typical cell culture medium has a homogenous electrolyte distribution and a potential gradient (field) that drives an ionic current through the medium. Consequently, each cell sees a different potential in its extracellular environment. Moreover, since the extracellular medium is much more conducting than the cell

[a] *Department of Chemical and Biomolecular Engineering, University of Notre Dame, Notre Dame, IN 46556, USA. E-mail: hchang@nd.edu, Pinar.Zorlutuna.1@nd.edu*
[b] *Center for Microfluidics and Medical Diagnostics, University of Notre Dame, Notre Dame, IN 46556, USA*
[c] *Department of Aerospace and Mechanical Engineering, University of Notre Dame, Notre Dame, IN 46556, USA*
[d] *Harper Cancer Research Institute, University of Notre Dame, Notre Dame, IN 46556, USA*

† Electronic supplementary information (ESI) available. See DOI: 10.1039/d0lc00809e

‡ Equal contribution.

membrane, very little field penetrates the cell membrane and most field lines circumvent the cells altogether. The induced voltage drop across most cells in earlier experiments with external fields is hence less than the approximately 20–50 mV required to activate or deactivate ion channels. Consequently, even though many of the studied phenomena (including various pathologies) are related to how voltage-gated ion channel activities affect the entire colony, actual studies of how a cell colony responds collectively to induced voltage across the membrane of each cell by an external field are under way.[22] In contrast, there is a huge body of voltage clamp studies of how cross-channel voltage changes the ion-channel conductance of a single cell, in the absence of any intercellular electrical communication or even single-cell autonomous action potential dynamics.[23–30] Additionally, a large focus for cardiotoxicity testing in drug development has been on the automation of this technology for high throughput drug discovery.[28,30–33] Unfortunately, these developments, in addition to testing on single cells, also only test a single ion channel, the human ether-a-go-go-related gene (hERG), and are inadequate in completely ruling out potentially toxic compounds prior to costly and time intensive dog telemetry studies.[34] Both the single ion channel and single-cell deficiencies of the voltage-clamp technique hence prevent in-depth study of how voltage-gated ion-channel pathologies and drugs are connected to dynamic intercellular communication in a multicellular culture. While external electrodes and external electrode arrays can influence and pace the cells, they cannot sustain a constant potential over the entire colony so that the ion-channel activities of the entire synchronized colony can be studied.

In this report, we introduce a novel non-invasive, flow-free and user-friendly technique to generate a high, uniform potential in the extracellular environment of an entire rCM colony by isolating the colony with low conductivity solutions. The steady-state and high-gradient ion concentration profile of a low conductivity buffer is imposed without external reservoirs and is sustained indefinitely by the ion-depletion action of a perm-selective membrane. Such a steady concentration gradient is otherwise difficult as the diffusion time is on the order of minutes for the dimension of a typical chip. Electric fields applied at the two ends of the ion-depletion zone enter and exit the high-conductivity colony without Joule heating or a significant current and the colony maintained a constant (tunable) voltage. The polarity of the extracellular voltage at the colony can also be changed, if the perm-selective membrane is replaced by one with opposite selectivity. In the current report, we only apply a positive extracellular voltage with a cation exchange membrane (CEM). Instead of using Nafion or other monolithic membranes synthesized *in situ*,[35–37] we cut pieces from commercial desalination membranes and assemble them into our chips. We have previously used such low-cost membrane-based microfluidic devices to induce depletion action for pH actuation, analyte concentration/isolation and molecular sensing.[38–41] The electric field in the depleted region is as high as 100 V cm^{-1}, higher than any previously published DC or AC exogenous fields, but with a relatively low current (~100 s μA, ~sub mW) to minimize Joule heating. This novel synchronization technique demonstrates significant usability not only in its ability to rapidly synchronize entire cardiac colonies demonstrated in this study, but also potentially in the field of drug development to bridge the gap between high throughput hERG voltage-clamp studies and low throughput costly dog telemetry studies. Additionally, this technique can provide useful insight into cardiac development and human induced pluripotent stem cell (hiPSC) derived cardiomyocyte (iCM) and neuron maturation.

Materials and methods

Microfluidics and device fabrication

Wax mold printing. The mold was designed in SolidWorks 2017 software (Dassault Systemes SolidWorks Corporation, USA) and was transferred as an STL (stereolithography) file to a wax 3D printer (Solidscape Studio-Solidscape, Inc.). A sacrificial layer (melt/dissolvable wax (Solidscape, Inc.)) was made around the main structure (Midas castable material (Solidscape Inc., USA)) to prevent mold breakage during post processing. Once the print job is completed, the print bed is removed from the printer and placed on top of a hotplate for 1 hour at 75 °C to loosen the wax mold for subsequent detachment. The sacrificial wax layer was then dissolved in BIOACT VSO (Vantage Specialty Chemicals) solvent for 2 days. When the sacrificial layer is fully dissolved, the devices are removed from the solvent and carefully wiped clean with narrow fiber paint brushes. They are then immersed in USP grade white mineral oil for the removal of trace amounts of VSO, and then rigorously air dried with an air blower.

PDMS device fabrication. A 1 : 10 weight ratio of curing agent and polydimethylsiloxane (PDMS, Sylgard 184, Dow Corning) base was mixed thoroughly and then degassed for 30 minutes to remove air bubbles. PDMS was then poured into the previously described molds and degassed again to remove any trapped air bubbles, followed by overnight curing at 35 °C. After curing, the wax print was removed by washing with dimethyl sulfoxide (manufacturer) (DMSO) for 3 hours to completely dissolve the wax mold. To remove the DMSO residual from the PDMS, isopropanol (IPA) was sprayed onto the PDMS. The DMSO was then thoroughly removed and a 1 mm biopsy punch was used to punch inlets and outlets. Both the device surface and 25 × 75 mm glass slides (Ted Pella, USA) were rinsed with IPA, dried, and then placed into a plasma cleaner (Harrick-Plasma PDC-001, USA) for 2 minutes for air plasma treatment. Following air plasma treatment, the devices were bonded together and incubated overnight at 80 °C.

Neonatal rat cardiomyocyte isolation. Animal studies were approved by the Institutional Animal Care and Use Committee at the University of Notre Dame. The animal procedures conformed to the NIH Guide for the Care and Use of Laboratory Animals. Neonatal rCMs were isolated from

2 day old rats (Sprague-Dawley, Charles River Laboratories) using a previously established protocol.[42] Briefly, the pups were anesthetized with isoflurane followed by immediate decapitation and excision of the heart. The hearts were then digested and ventricular cardiomyocytes were isolated and seeded into the microfluidic device as described.

Device seeding. Prior to rCM isolation, the devices were washed with PBS (VWR, USA) and sterilized under UV light for 30 minutes. The devices were then incubated with fibronectin (50 μg mL^{-1}) (Sigma Aldrich, USA) for 30 minutes at 37 °C. After incubation, custom made PDMS blockers were inserted into the two large reservoirs and outlets in the depletion channel to localize rCM attachment to the seeding channel. Following blocker placement, the devices were washed with fresh, filtered DMEM supplemented with FBS (10%) (Hyclone, USA) and penicillin (1%) (Sigma Aldrich, USA). Finally, the devices were placed in a Petri dish containing 1.5 mL of PBS supplemented with penicillin (5%) and stored until seeding.

Following rCM isolation, 20 μl of the cell suspension (~150 000 cells) were seeded into each device. The devices were then cultured overnight under normal incubation conditions (37 °C, 21% O_2, 5% CO_2) to allow for cell attachment. The next day, cell attachment was confirmed and the medium was changed to remove any cell debris and/or dead cells remaining in the device. The devices were then imaged using a Zeiss Axiovert 200M fluorescence/live cell imaging inverted microscope.

Voltage measurement. In order to perform voltage measurements within the microfluidic device, a new 3D printed mold was designed and manufactured as described above. Two different aluminum wires were attached to the junction of the seeding and depletion channel, respectively, to measure the voltage drop across the ends of the connecting channel. To perform voltage measurement tests, the wires coming from the two ends were connecting to a digital multimeter (34401A Agilent Multimeter, USA). The data were recorded using BenchVue software (Keysight Technologies, USA).

Experimentation

Electrical stimulation. CEMs with negative charge due to organosulfate groups were procured from Mega a.s. (Czech Republic). Membrane reservoir fabrication was performed as described previously.[43] Briefly, a small piece of the CEM (~10 mm^2) was embedded in a two component fast curing resin (TAP Plastic Inc., USA) in a 1 : 1 ratio for 30 minutes in a custom designed mold in a two component silicon RTV system (TAP Plastic Inc.). After releasing the mold, a hollow cylindrical structure with an exposed CEM surface was obtained. The membrane was kept in a microcentrifuge tube (Argos Technologies, USA) filled with phosphate buffered saline (PBS) (Fisher Scientific, USA) for overnight swelling followed by overnight UV sterilization. While performing the experiments, the membrane reservoir was gently pushed inside the PDMS device seeded with rCMs. For the other reservoir, 1000 μl pipette tips (VWR, USA) were cut with a razor blade and were gently pushed to create a seal with the PDMS and filled with cell medium. The cell medium was then subsequently changed to remove any trapped bubble during the process and was kept under normal cell culture conditions for 30 minutes. The device was then placed in a sterilized Zeiss stage incubator, under standard culture conditions, and incubated for 20 minutes to achieve synchronous beating. For stimulation tests with the CEM, two platinum electrodes were inserted into the device, with the negative electrode placed in the membrane reservoir and the positive in the open reservoir. For no membrane studies, the two open reservoirs were filled with cell medium and electrodes were placed in them. Voltage was then applied using a DC power supply (Biorad PowerPac Basic Electrophoresis Power Supply, USA) and current was observed using a digital multimeter (34401A Agilent Multimeter, USA). A voltage of 45 V was chosen and is applied throughout the paper unless otherwise mentioned. All videos were recorded at 30 fps.

Video analysis. The video files were converted from ZEN files to .avi, which are subsequently analyzed *via* a custom written image analysis code in Matlab based on previously published algorithms.[7,44] The approach is based on the analysis of the change in pixel intensity in a bright field video over time with respect to its subsequent frame. Parameters for illumination for optical microscopy were optimized before taking a video. Fig. 1(e) shows a representative trace of rCM contraction extracted from image analysis. The raw trace was normalized to its mean value during the analysis time interval. The obtained time series was then further analyzed to obtain various time scale parameters such as the peak to peak time, contraction time (CT), relaxation time (RT), contraction–relaxation duration (CRD), number of peaks, normalized maximum contraction speed (MCS) and normalized maximum relaxation speed (MRS). The beating frequency was calculated by dividing the obtained number of contraction peaks by the duration of the observation period. Each experimental trace of beating frequency was normalized to its initial 10 s value to quantitatively represent the progression of beating frequency in each experiment. The onset of contraction denotes the time point when the intensity is 10% above its difference from the peak amplitude and its baseline value. The CT is then calculated as the difference between the onset time till the velocity becomes minimum. The RT is also calculated in a similar fashion. The end of relaxation is marked as the 90% reduction in its amplitude value with respect to its baseline value. The CRD was then calculated by summing both the CT and RT. "Image correlated field potential duration" was defined as the time interval between the onset of contraction and the peak of relaxation motion.

Immunohistochemistry. Standard immunohistochemistry staining was performed. Briefly, rCMs were fixed with 4% paraformaldehyde (Electron Microscopy Sciences, USA) for 30

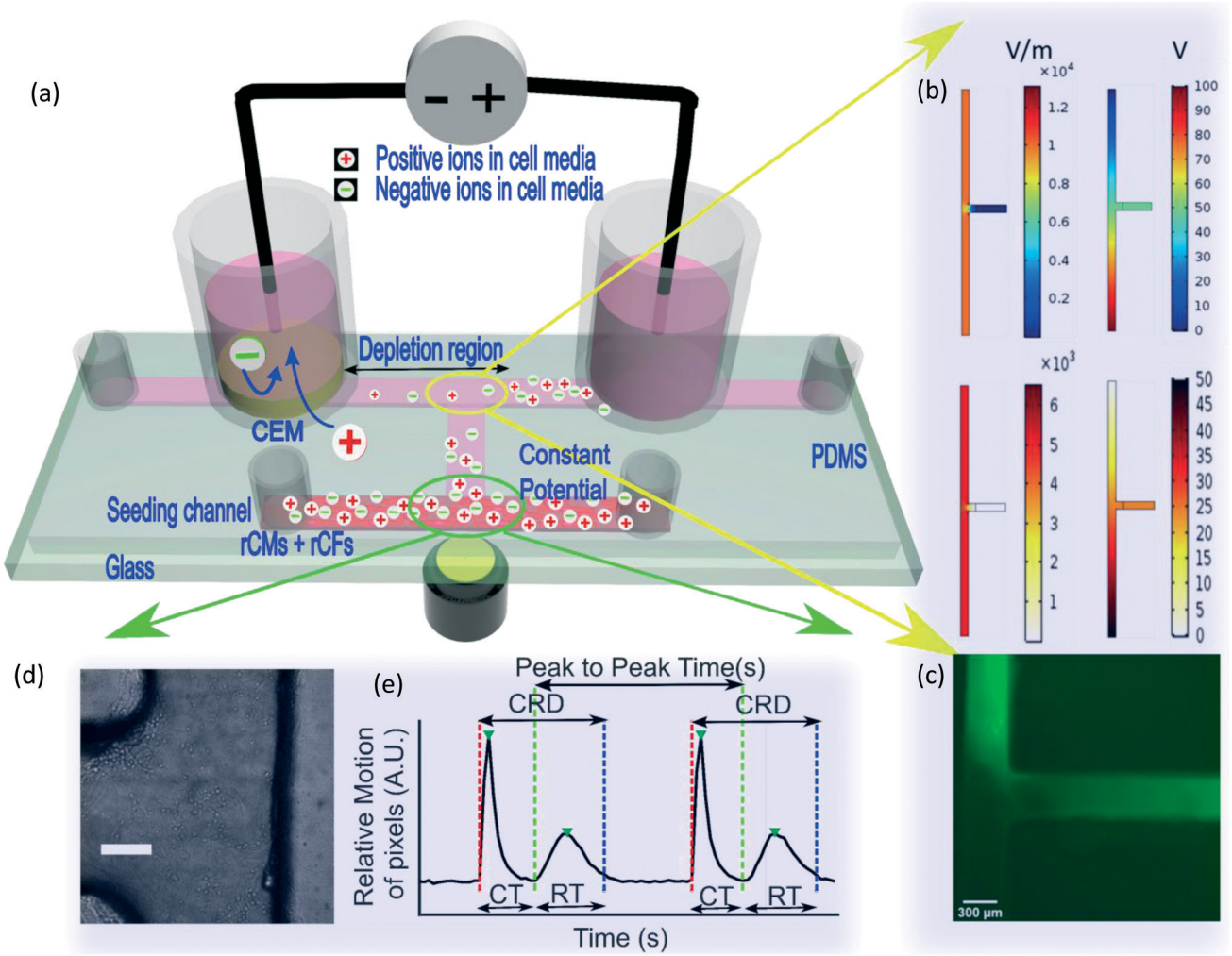

Fig. 1 Overview of the experimental platform. (a) Schematic representation of the experimental setup. (b) Finite element simulation results of field and potential in the zoomed section showing a uniform potential in the cell colony. (c) A picture of the chip showing the location of the depletion front developed by the applied field. A negatively charged fluorescein dye is used to track the depletion front. Scale bar represents 300μm. (d) A bright field image of the region where rCMs are seeded (scale bar is 100μm) and (e) a representative trace obtained by image analysis and time series analysis.

minutes followed by permeabilization with 0.1% Triton-X (Thermo Fisher Scientific, USA) for 15 minutes. Samples were then blocked and then incubated with cardiac troponin T (Abcam, USA) and HCN2 (Abcam, USA) primary antibodies overnight at 4 °C. After primary antibody incubation, samples were then incubated with secondary antibody for 6 hours at 4 °C followed by DAPI staining for 10 minutes at room temperature. Samples were then imaged with a Zeiss Axio Observer.Z1 fluorescence microscope and processed with Zeiss Zen software.

Statistical analysis. The data in this study have been presented as mean ± standard error of the mean (S.E.M) unless otherwise specified. For box and whisker plots, the whiskers represent the SEM. The obtained data were compared with either a two-sample *t* test or, for experiments with more than two sample groups, a one-way ANOVA with Tukey's *post hoc* test and the value of $p < 0.05$ was considered significant.

Results and discussion

Fig. 1 shows the overall device design and predicted and measured voltage drops at distinct regions of the device. We deplete the ions in the straight channel shown in Fig. 1(a). The cells are seeded in a parallel channel and are connected to the first depletion channel by a side channel. This field potential is still lower than the threshold field required to damage molecules such as DNA or proteins present within the cell culture and medium (tens of kV cm^{-1}).[45] Because of the electrode placement, our simulation of the leaky dielectric model of electrolytes in Fig. 1(b) shows that depletion occurs only in the depletion channel. The field is negligible in the cross channel and the cell colony sees a uniform potential that can be controlled *via* the applied voltage.

The depletion channel contains a CEM embedded in polyurethane resin and a reservoir for applying voltage. All

the experiments were performed by generating a depletion front in the depletion channel whereas ion enrichment experiments caused the current in the circuit to rise past 3 mA resulting in cell death. Fig. 1(c) shows the extent of depletion through the use of a charged fluorescence dye solution. It is shown to extend slightly into the connecting side channel but not into the cell channel, as is consistent with our simulation. Fig. 1(d) represents the bright field image of the region of interest, at the junction between the side and cell channels. Fig. 1(e) is a schematic of the time series obtained from image analysis described in detail in the Experimentation and Video analysis sections.

The beating motion of rCMs in a small neighborhood was observed *via* time-lapse imaging (see ESI† Video S1). The rCMs exhibit first a contraction peak followed by a relaxation peak and then a long stationary transient is observed before the twin peaks appear again. As shown by Hayakawa *et al.*,[46] the contraction phase is related to the depolarized plateau phase and the relaxation phase occurs during the hyperpolarization phase (see Fig. S1†). To facilitate fabrication of the required multilayer structure design, a 3D-printed meltable wax mold was used to fabricate smooth 300 μm wide channels. Fig. S3† shows the fabrication process which is described in detail in the Microfluidics and device fabrication section.

To demonstrate that the cell channel is under a uniform potential, we measure the voltage drop across the connecting side channel in two chips as shown in Fig. 2(a), one with and the other without the CEM. Fig. 2(b) and (c) depict the measured voltage in response to irregular 'ON' and 'OFF' switching of the voltage. With the CEM, a characteristic RC transient after voltage activation leads to a constant voltage drop. Without the membrane, a constant potential is never reached in the cell colony. Instead, rapid fluctuations are observed, quite possibly due to microbubble formation and faradaic reactions, which are expected beyond 10 V.[47] Depletion action by the CEM has hence eliminated such fluctuations and produced a constant potential in the cell channel.

Effect of voltage on rCM beating dynamics

Fig. 3 shows the effect of the uniform potential microenvironment on beating rCMs during the first five minutes of application through the CEM. The rCMs start responding to the elevated extracellular potential instantaneously. This is evident from the normalized contraction–relaxation trace obtained from image analysis as presented in Fig. 3(a) showing a discernable difference in the time series before and immediately during the application of voltage. Some reduction in the width of both the contraction and relaxation peaks is also evident. In order to better visualize the transient, the normalized beating frequencies were calculated after every 10 s and plotted against time as shown in Fig. 3(b). For the initial 30 s, no voltage was applied, and the voltage was turned on subsequently after that for the rest of the five minute recording. Under the influence of the applied external field, the beating frequency increased and then saturated at around 3 minutes for the stimulated cases. The beating frequency remained roughly stable for the next two minutes at a higher beat rate than the original beating frequency (2.23 ± 0.52-fold change compared to the baseline). The control transient trace shown in Fig. 3(c) represents the unstimulated control sample when no voltage was applied to the setup and approximately maintained its original value till the end of the five minute recording window. Most striking is the separation of the contraction/relaxation twin peaks reduces significantly as seen in Fig. 3(d).

To explore the effect of spatial uniformity of the extracellular potential introduced by the depletion action of the CEM, a voltage was applied without using the CEM. A potential of 45 V was unsuccessful as Joule heating caused permanent damage to the cells within five minutes of field induction. In order to perform a control study without the CEM, the device was operated at a constant current. The current through the CEM saturated in the range of 0.1–0.7 mA during the first five minutes and a higher end current, *i.e.* 0.7 mA, was used for the control study as shown in Fig. 3(c). In these experiments without the CEM, synchronized beating was not observed and the beating profile of the cells was unstable and irregular. The beating frequency in two of the no membrane control studies decreased below its initial value till the end of the five minute time period while it was highly unstable in the other one as shown in Fig. 3(e). This "counter example" highlights the effect of non-uniform potential. Without the depletion, the potential varies significantly across the cell colony and synchronization becomes impossible.

Since the beating rate stabilizes within the first three minutes of voltage application, the beating dynamics can be contrasted to better understand the effect of a high extracellular potential on the rCMs. An arbitrary 30 s time interval (210–240 s) was chosen when the beat rate was stable and contrasted against the first 30 s when no electric field was applied. As shown in Fig. 3(d), the RT and CT both decrease appreciably compared to when no field was applied. In Fig. 3(e), the significant difference in the peak-to-peak CRD durations of the cells at equilibrium in the polarized phase is also apparent in Fig. 3(a). These effects were not

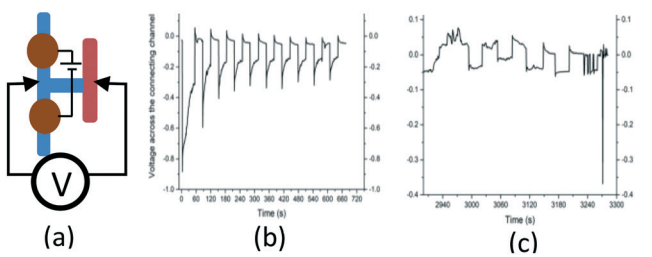

Fig. 2 Voltage drop measurement across the connecting channel. (a) Schematics of the voltage measurement setup and observed voltage change across the side channel with (b) and without (c) a CEM.

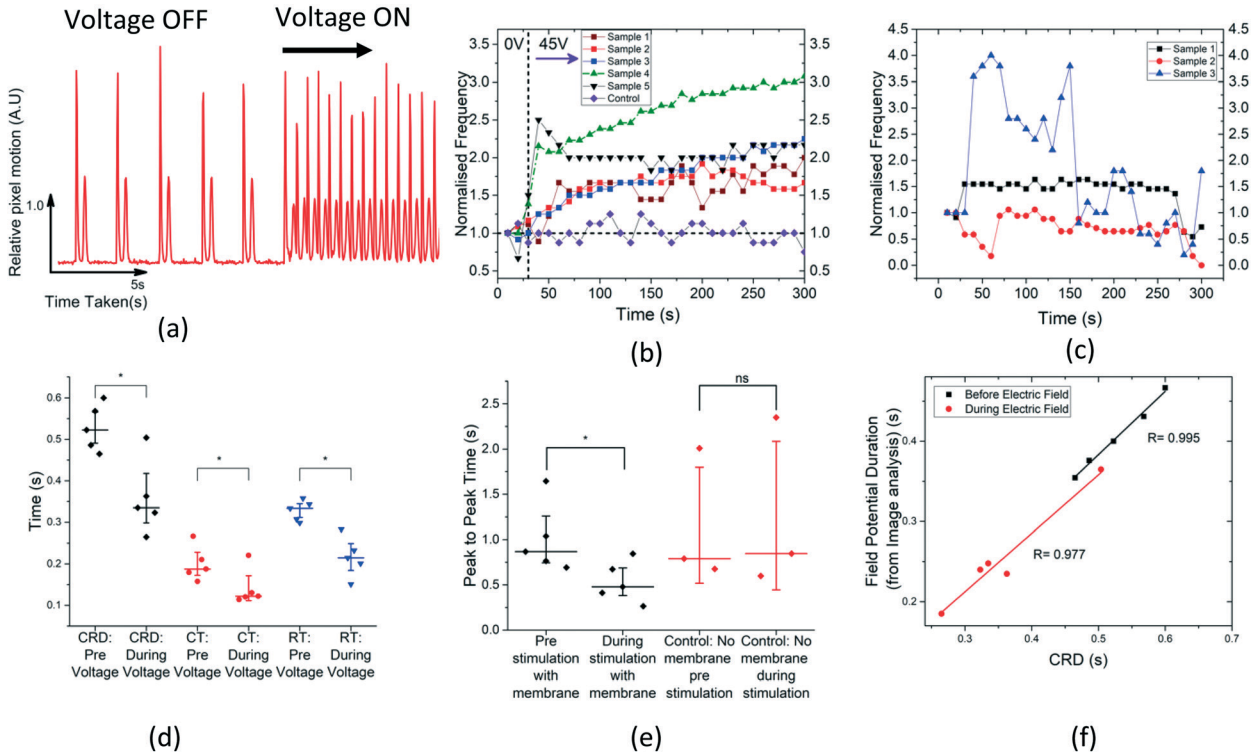

Fig. 3 Effect of voltage on the time scales of uniformly beating rCMs with and without a CEM during first five minutes of the depletion. (a) The trace evaluated from image analysis depicting the abrupt transition when voltage is turned on. (b) The beating frequency transient. The beating frequency is normalised by dividing the frequency obtained in each 10 s interval with its initial 10 s value (n = 5). (c) The beating frequency transient in the control study without using a membrane (n = 3). (d) The comparison of total time taken to complete an oscillation, CT and RT scales before applying voltage (0–30 s) and during the application of voltage (210–240 s) for a 30 s time interval in all cases (*$p < 0.05$). (e) The peak to peak time before and during the electrical stimulation (*$p < 0.05$). (f) Correlated field potential duration (onset of contraction to relaxation peak) obtained from image analysis *vs.* the total contraction–relaxation time CRD taken for a beat indicates that contraction initiation dynamics is reduced in duration in proportion to the full contraction duration.

observed without the CEM. To establish that the depolarization cycle is self-similar, the image correlating the applied potential duration between the onset of contraction and the relaxation peak was plotted against the CRD between peaks in Fig. 3(f) and a good linear and near-identical correlation was observed during the "off" (R = 0.995) and "on" (R = 0.977) states. This suggests that the entire depolarized phase is reduced in duration due to voltage-gated activities.

We are able to form a hypothesis on ion-channel mechanisms from the dynamics triggered by uniform constant potential. From voltage clamp experiments, a positive extracellular potential (or a negative intracellular potential) is known to activate HCN ion channels and deactivate all other calcium, sodium and potassium channels, for cardiomyocytes, Fig. 4(a).[48–54] In prior voltage clamp and drug activation/inhibition experiments on voltage-gated ion channel conductance, the duration of the long polarized interval between the twin contraction/relaxation peaks, when the cell is in equilibrium and motionless, is reduced by activating HCN ion channels to trigger depolarization sooner and the width of the depolarized plateau is shortened by deactivating L-type Ca_v ion channels which sustain a positive membrane potential.[46,55–58] Our observation that the peak-to-peak time is reduced by a factor of two and the contraction and relaxation intervals are also reduced is consistent with activated HCN and deactivated L-type Ca_v channels by a positive extracellular potential. This suggests that these channels may be more sensitive to a positive external potential than other cardiac related ion channels.

As the HCN channel is the only channel that is activated by a positive external potential based on the literature from single-cell voltage clamp experiments, and it might be chiefly responsible for the duration of the polarized phase with a negative membrane potential,[57,58] we suggest that these observations are at least partially due to activation of the HCN2 channels, Fig. 4(b). In this study, we confirmed the existence of HCN2 channels in our neonatal rCM cells in Fig. 4(c and d) *via* immunostaining. In future studies, we will look to further confirming this observation with drug-activated HCN studies.

We are able to confirm that drug-deactivated Ca_v ion channels reduce the peak-to-peak contraction and relaxation CRD durations and amplitudes during the depolarized phase with respect to controls by analyzing the existing literature[46,55,59–61] as presented in Fig. 4(a). No other drug activated or deactivated ion channels examined in the

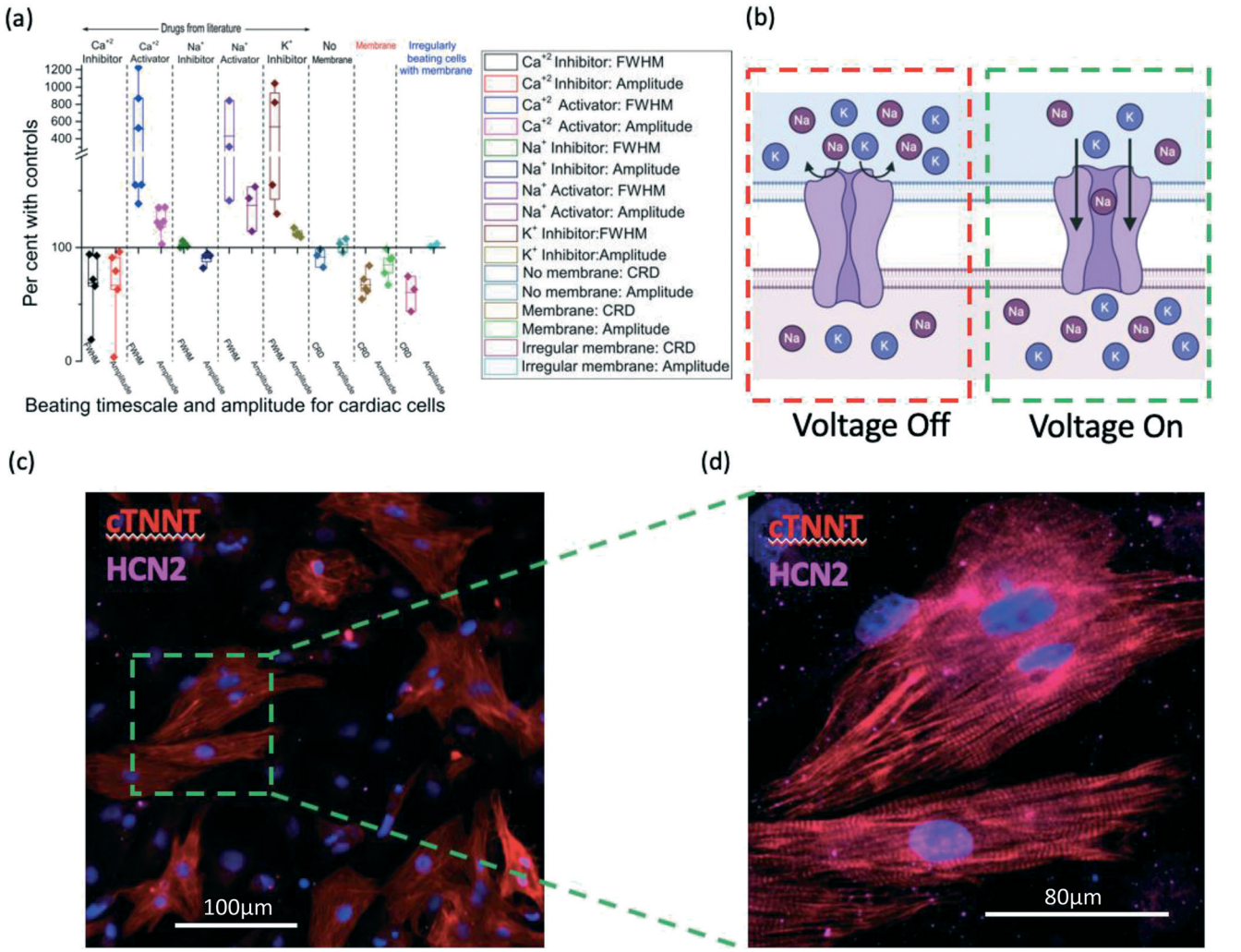

Fig. 4 (a) Comparison of cardiomyocyte motion kinetics with the literature (ref. 46, 55 and 59–61) depicting the effect of voltage gated ion channel agonists/antagonists. [FWHM (full width at half maximum), roughly corresponding to the CRD peak-to-peak time between contraction and relaxation, is from the trace obtained by using calcium dye (Fluo-4) and CRD is the contraction–relaxation time obtained from bright field video analysis.] (b) Cartoon schematic of an rCM HCN2 channel with the voltage turned off (closed) and on (open). (c and d) rCMs stained for cardiac troponin t (cTTNT, red) and HCN2 (magenta).

literature show this particular feature. The amount of reduction in both the CRD duration and amplitude of these two peaks is comparable to our data qualitatively. This suggests that we can mimic drug deactivation of Ca_v ion channels with our uniform positive potential on the entire rCM colony. This timescale of milliseconds is a much more rapid assay than drug induced studies which typically induce a response on the scale of seconds to minutes. It should be noted that the data taken from the literature shown in Fig. 4(a) have high variability and experiments were performed in different devices. However, we have utilized them to solely develop a qualitative estimate of the rCM behavior. Complete testing of the hypothesis requires very extensive and detailed experimentation which is beyond the scope of the current manuscript. These suggested mechanisms are proof-of-concept studies to show the usefulness of our technology.

Effect of uniform potential on colony synchronization

Our data also suggest that we are enhancing rCM synchronization with the applied uniform extracellular potential, which would be consistent with potential activation of the HCN ion channels. Our first observation on synchronization was seen during the first five minutes of voltage induction: application of voltage using the CEM synchronized the beating rate of otherwise irregularly beating rCM clusters into a single frequency. These rCM clusters were beating sporadically and stopped intermittently. When they did beat, there was local synchrony but not throughout the entire colony. The contraction–relaxation trace obtained from image analysis for the entire recorded time period of one such case is displayed in Fig. 5(a) where the irregularly beating cells are stabilized by the uniform potential during the first recorded five minutes. The corresponding beat rate

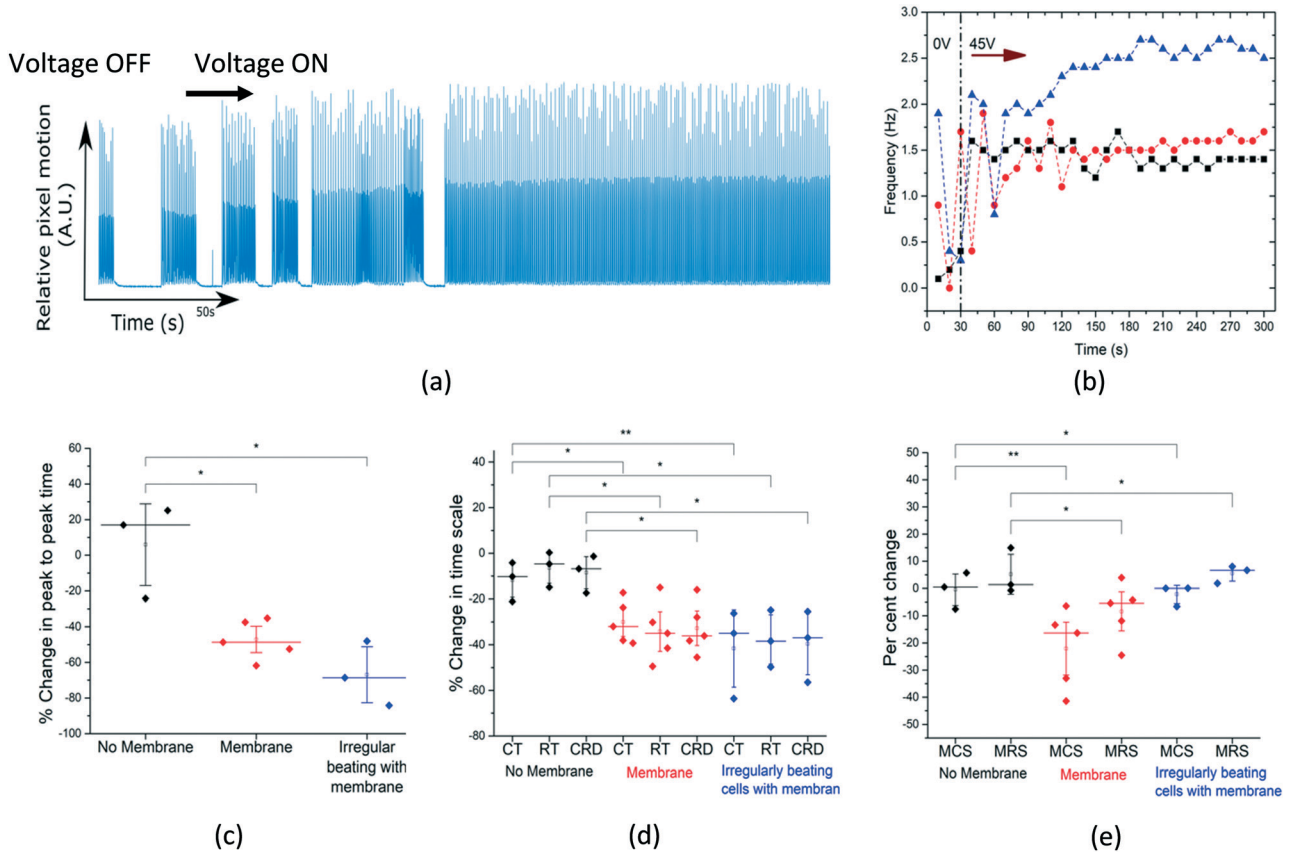

Fig. 5 Irregularly beating cells with regular beats during electrical stimulation and comparative studies. (a) Trace of the entire event. Depicting sporadic beats which stabilized within minutes after the application of voltage. (b) The beating frequency transient showing that the rCMs were beating intermittently. Application of voltage after 30 s of recording showed that they stabilized and saturated at an elevated beating frequency. (c) The percentage change in peak to peak time before and during the experiment between the no membrane control, membrane and irregularly beating cells with the membrane. Two-sample *t* test was performed (*$p < 0.05$). (d) The percentage change in CT, RT and contraction relaxation duration before and during the experiment between the no membrane control, membrane and irregularly beating cells with the membrane. Two-sample *t* test was performed (*$p < 0.05$, **$p < 0.1$). (e) The percentage change in maximum contraction speed and maximum relaxation speed: before and during the experiment between the no membrane control, membrane and irregularly beating cells with the membrane. Two-sample *t* test was performed (*$p < 0.1$, **$p = 0.556$).

is displayed in Fig. 5(b) where the beating frequency was highly irregular before applying voltage. Turning on the voltage stabilized the beating frequency roughly during the first three recorded minutes. For comparison, the percentage change in the time scales in the 30 second interval before applying voltage and 30 seconds (210–240 s) afterwards was calculated for all the cases: voltage without the membrane, voltage with the membrane and voltage with the membrane on irregularly beating cells in Fig. 5(c and d). Fig. 5(e) shows that a significant percentage change in the peak to peak time was observed between the cases when the ion exchange membrane was present as compared to the one without it. The CT and RT time scales also showed a significant difference between the no-membrane cases as compared with the cases presented with the membrane. The percentage change in beat velocities for both relaxation and contraction was not significant for the cases with electrical stimulation with the membrane as compared to the control samples without the membrane. It is hence quite clear that the uniform potential introduced by the depletion action of the CEM significantly increases synchronization over the entire colony. As demonstrated in Fig. 4c and d, both the isotropic and non-uniform nature of the rCMs potentially hinder the synchronization efficiency of the constant-potential environment created using the ion depletion technology. There is extensive evidence in the literature that an anisotropic environment promotes enhanced electrical signaling and subsequent cardiomyocyte maturation both in rCMs and iCMs.[62–69] Similarly, the non-uniform nature of the rCM culture due to the inclusion (and subsequent proliferation) of cardiac fibroblasts which have been shown to significantly alter, and when present in larger quantities, potentially decrease signal propagation.[70–73] An increase in the rCM: fibroblast ratio could rectify this, as the inability of fibroblasts to trigger their own action potential and their propensity to dampen any signal passed through due to their internal resistance could potentially decrease ion movement between rCM clusters in the culture. Future studies will focus on these factors and the role they play both in the developed system itself and in cardiomyocyte maturation.

hiPSCs have over the past decade established themselves as a promising cell resource for the study of human cardiac development and disease. Unfortunately, their use is hindered by issues regarding cell maturity and differentiation efficiency that prevent obtaining results directly mimicking what is seen clinically.[14,74–78] Long term AC stimulation of iCMs has shown promise as both a maturation and differentiation technique but has proven inadequate in definitively maturing iCMs to an adult phenotype.[11,14] The stimulation method developed in our study demonstrates for the first time, to our knowledge, the effect of the DC electric field on cardiomyocyte autonomous synchronization. This rapid synchronization technique demonstrates great promise to enable novel studies to better promote iCM differentiation efficiency, maturation, and synchronization that will be further investigated in future studies.

On demand switching of synchronized beating with uniform potential

We observed an interesting event when the voltage was continuously applied to the rCMs in the microfluidic chip. As the depletion front approaches the junction of the depletion channel, a localized change in the ionic strength occurs. In order to check the synchronous behavior of the cells and their spatial variations, four different spatial regions were identified as shown in Fig. 6(a). A binary mask was generated for each of these regions of interest and subsequent image analysis was performed on them one at a time. The trace obtained from image analysis from each of these four spatial locations is shown in Fig. 6(b). The trace profiles reveal that the cells were beating 'on command' with the applied voltage. No phase difference or delay in the onset of contraction and relaxation was observed. As shown in Fig. 6(b), the 30 s time period of square pulse voltage was applied five times. Every time rCMs responded to the applied electric field and stopped and started beating synchronously. As shown in Fig. 6(c), when the voltage was on at 45 V, rCMs were beating synchronously and smoothly. When the voltage is turned off after 30 s, the entire cluster stopped beating, with beating resuming at a higher frequency when the electric field was turned back on. The CT and RT show a decrease in their absolute values when the applied potential

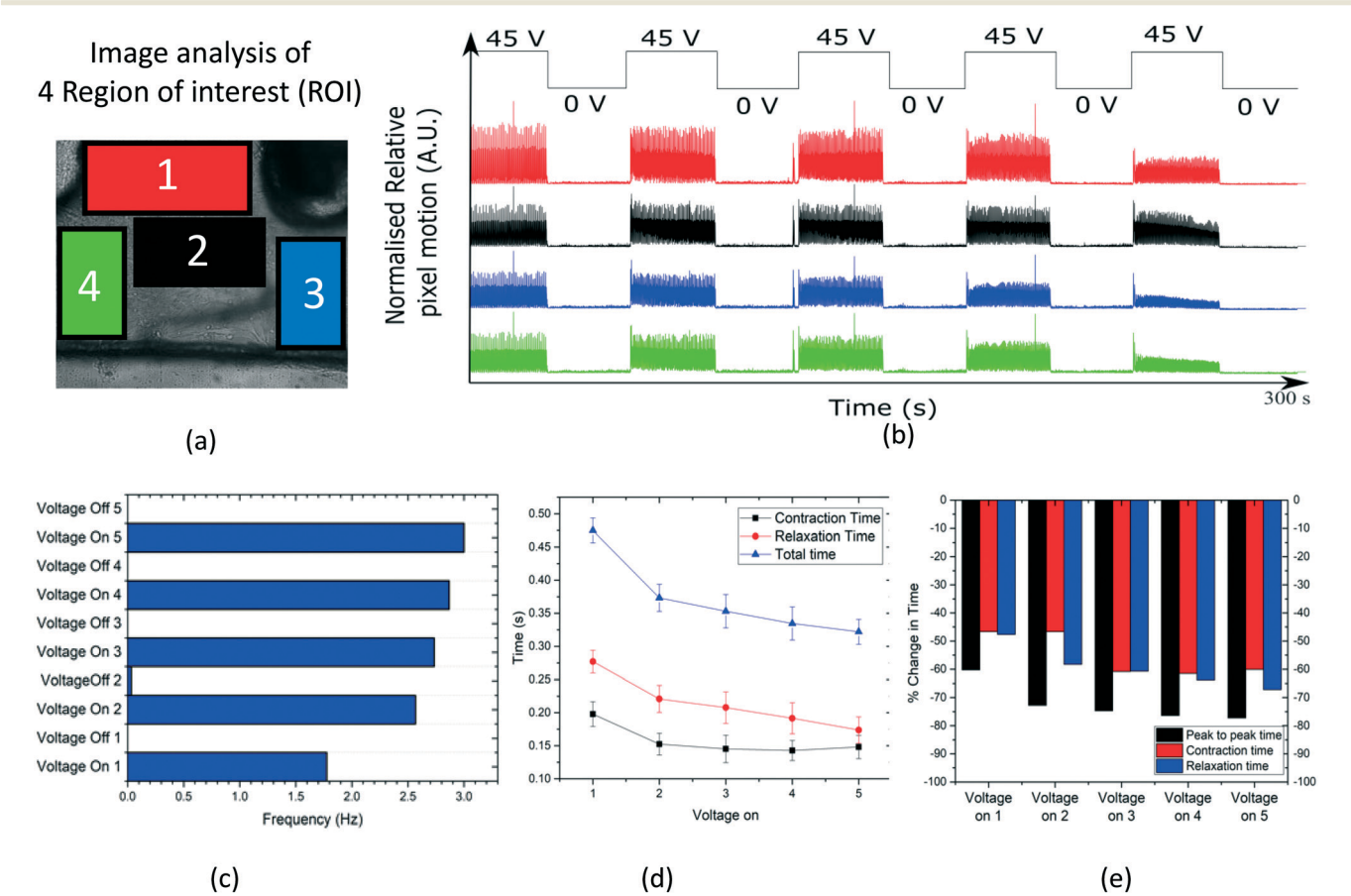

Fig. 6 On command synchronization of cardiomyocytes with the applied voltage pulse. (a) A snapshot of the image of the cells at the junction of the connecting channel and the cell channel. Four different spatial regions of interest (ROI) were identified for subsequent image analysis. (b) The trace obtained from 4 ROIs and their behaviour with ON/OFF applied field. (c) The beating frequency each time when the voltage is switched ON and OFF. (d) The contraction (CT), relaxation (RT) and total (CRD) time to complete a beat during the time when the voltage in ON. Error bars are the standard deviation for the respective time scale. (e) The percentage change in the relaxation, contraction and total time with respect to its pre-recorded value for each time when the voltage is switched ON.

was switched on as evident from Fig. 6(d). The percent change was calculated in the peak-to-peak time scale, CT and RT with respect to the case when no voltage was applied to it. 70% reduction in peak-to-peak time was observed while for other time scales (contraction and relaxation) more than 50% reduction was observed as shown in Fig. 6(e).

A constant high DC potential in an extracellular environment to activate ion channels synchronously over the entire colony can offer invaluable insight into the electric coupling of neurons and cardiac cells. In neuron communication, extracellular charge generation due to ion channel fluxes has long been speculated to produce extracellular potentials that are far stronger than the action potential of a single neuron. This extracellular charge and potential has been hypothesized to be responsible for long-range synchronization of neuron cells by a mechanism termed "ephaptic coupling".[79] A strong cloud of extracellular charge, released by a localized subset of synchronized cells, can produce far-reaching fields to recruit other cells to fire their ion channels synchronously. Long-range synchronization of cerebellar Purkinje cells, for example, has been attributed to this external field mechanism.[80] These observations demonstrate that potentially, neighboring cell communication can differ from global synchronization, with disparate time scales and potential amplitudes. It has yet to be established, to our knowledge, if such an external ephaptic coupling mechanism exists within the heart and its potential relevance to the cardiovascular physiology. The on-chip system developed in this study will enable such new mechanisms to be studied for cardiac tissue and beyond.

Conclusions

In conclusion, we have used a permselective membrane on a chip to produce a uniform potential over an entire colony of rCMs, such that each cell in the colony sees the same elevated extracellular potential. From image and time series analysis, we see evidence that the uniformly applied external potential potentially synchronously deactivates L-type Ca^{2+} and activates HCN voltage gated ion channels. The former effect produces a similar reduction in the contraction and relaxation durations to drug-deactivation studies. Three novel synchronization phenomena were observed: a rapid on command synchronization of rCMs with the applied external potential, the ability to reversibly stop rCMs from contracting completely, and the ability to normalize irregular beating frequencies. Enabling voltage-gated channel activities synchronously over the entire communicating colony, without the use of voltage clamps, could allow better characterization of ion channel related pathology and drug effects on cell communication and synchronization, bridging the gap between the high throughput, but relatively narrow automated voltage clamp technologies and high cost, time intensive dog telemetry studies. We believe that such collective feedback induced by the constant potential microenvironment should also be invaluable in training pluripotent stem cells into cardiomyocytes or neuronal colonies with high connectivity.

Conflicts of interest

There are no conflicts of interest to declare.

Acknowledgements

The present work is supported by the National Science Foundation (NSF) ECCS-1807551, Semiconductor Research Corporation (SRC) GRC TASK 2840.001, and the Naughton Fellowship.

References

1 L. P. da Silva, S. C. Kundu, R. L. Reis and V. M. Correlo, *Trends Biotechnol.*, 2020, **38**, 24–49.
2 J. Hunckler and A. de Mel, *J. Multidiscip. Healthc.*, 2017, **10**, 179–194.
3 R. Wever, *Int. J. Biometeorol.*, 1973, **17**, 227–232.
4 K. M. C. Oliveira, J. H. Barker, E. Berezikov, L. Pindur, S. Kynigopoulos, M. Eischen-Loges, Z. Han, M. B. Bhavsar, D. Henrich and L. Leppik, *Sci. Rep.*, 2019, **9**, 11433.
5 A. Gothelf, L. M. Mir and J. Gehl, *Cancer Treat. Rev.*, 2003, **29**, 371–387.
6 S. S. Nunes, J. W. Miklas, J. Liu, R. Aschar-sobbi, Y. Xiao, B. Zhang, J. Jiang, S. Massé, M. Gagliardi, A. Hsieh, N. Thavandiran, M. A. Laflamme, K. Nanthakumar, G. J. Gross, P. H. Backx, G. Keller and M. Radisic, *Nat. Methods*, 2013, **10**, 781–787.
7 N. Tandon, C. Cannizzaro, P. H. G. Chao, R. Maidhof, A. Marsano, H. T. H. Au, M. Radisic and G. Vunjak-Novakovic, *Nat. Protoc.*, 2009, **4**, 155–173.
8 E. Holt, P. K. Lunde, O. M. Sejersted and G. Christensen, *Basic Res. Cardiol.*, 1997, **92**, 289–298.
9 A. Grosberg, P. W. Alford, M. L. McCain and K. Kit Parker, *Lab Chip*, 2011, **11**, 4165–4173.
10 H. J. Berger, S. K. Prasad, A. J. Davidoff, D. Pimental, O. Ellingsen, J. D. Marsh, T. W. Smith and R. A. Kelly, *Am. J. Physiol.*, 1994, **266**, H341–H349.
11 R. Balint, N. J. Cassidy and S. H. Cartmell, *Tissue Eng., Part B*, 2012, **19**, 48–57.
12 L. L. Y. Chiu, R. K. Iyer, J.-P. King and M. Radisic, *Tissue Eng., Part A*, 2011, **17**, 1465–1477.
13 N. Tandon, A. Marsano, R. Maidhof, L. Wan, H. Park and G. Vunjak-Novakovic, *J. Tissue Eng. Regener. Med.*, 2011, **5**, e115–e125.
14 K. Ronaldson-Bouchard, K. Yeager, D. Teles, T. Chen, S. Ma, L. Song, K. Morikawa, H. M. Wobma, A. Vasciaveo, E. C. Ruiz, M. Yazawa and G. Vunjak-Novakovic, *Nat. Protoc.*, 2019, **14**, 2781–2817.
15 X. Sun and S. S. Nunes, *Methods*, 2016, **101**, 21–26.
16 N. Tandon, A. Marsano, R. Maidhof, L. Wan, H. Park and G. Vunjak-novakovic, *J. Tissue Eng. Regener. Med.*, 2011, **5**, 115–125.
17 D. J. Dosdall, V. G. Fast and R. E. Ideker, *Annu. Rev. Biomed. Eng.*, 2010, **12**, 233–258.
18 P. X. de Oliveira, R. A. Bassani and J. W. M. Bassani, *IEEE Trans. Biomed. Eng.*, 2008, **55**, 2635–2642.

19 D. R. Merrill, M. Bikson and J. G. R. Jefferys, *J. Neurosci. Methods*, 2005, **141**, 171–198.
20 B. Cetin and D. Li, *Electrophoresis*, 2008, **29**, 994–1005.
21 C. Huh and M. H. Kim, *Exp. Therm. Fluid Sci.*, 2006, **30**, 775–784.
22 F. Lehmann-Horn and K. Jurkat-Rott, *Physiol. Rev.*, 1999, **79**, 1317–1372.
23 J. Cowgill and B. Chanda, *J. Gen. Physiol.*, 2019, **151**, 1163–1172.
24 W. A. Catterall, *J. Physiol.*, 2012, **590**, 2577–2589.
25 W. Zhu, Z. Varga and J. R. Silva, *Prog. Biophys. Mol. Biol.*, 2016, **120**, 3–17.
26 F. A. Ortega, E. Grandi, T. Krogh-Madsen and D. J. Christini, *Front. Physiol.*, 2017, **8**, 1099.
27 P. Imbrici, O. Nicolotti, F. Leonetti, D. Conte and A. Liantonio, in *Computational Toxicology*, Springer, 2018, pp. 313–326.
28 H. Huang, M. K. Pugsley, B. Fermini, M. J. Curtis, J. Koerner, M. Accardi and S. Authier, *J. Pharmacol. Toxicol. Methods*, 2017, **87**, 11–23.
29 A. Obergrussberger, S. Stölzle-Feix, N. Becker, A. Brüggemann, N. Fertig and C. Möller, *Channels*, 2015, **9**, 367–375.
30 C. Möller and H. Witchel, *Front. Pharmacol.*, 2011, **2**, 73.
31 T. Wang, X. Chen, J. Yu, Q. Du, J. Zhu, M. Yang, H. Wu, M. Wang and Y. Zhu, *Am. J. Chin. Med.*, 2018, **46**, 1825–1840.
32 Y. Haraguchi, A. Ohtsuki, T. Oka and T. Shimizu, *BMC Pharmacol. Toxicol.*, 2015, **16**, 39.
33 X. Li, R. Zhang, B. Zhao, C. Lossin and Z. Cao, *Arch. Toxicol.*, 2016, **90**, 1803–1816.
34 L. Ewart, M. Aylott, M. Deurinck, M. Engwall, D. J. Gallacher, H. Geys, P. Jarvis, H. Ju, D. Leishman, L. Leong, N. McMahon, A. Mead, P. Milliken, W. Suter, A. Teisman, K. Van Ammel, H. M. Vargas, R. Wallis and J. P. Valentin, *Toxicol. Sci.*, 2014, **142**, 427–435.
35 M. Kim, M. Jia and T. Kim, *Analyst*, 2013, **138**, 1370–1378.
36 S. H. Ko, Y. A. Song, S. J. Kim, M. Kim, J. Han and K. H. Kang, *Lab Chip*, 2012, **12**, 4472–4482.
37 S. J. Kim, Y. A. Song and J. Han, *Chem. Soc. Rev.*, 2010, **39**, 912–922.
38 Z. Slouka, S. Senapati and H.-C. Chang, *Annu. Rev. Anal. Chem.*, 2014, **7**, 317–335.
39 L.-J. Cheng and H.-C. Chang, *Lab Chip*, 2014, **14**, 979.
40 S. Marczak, K. Richards, Z. Ramshani, E. Smith, S. Senapati, R. Hill, D. B. Go and H.-C. Chang, *Electrophoresis*, 2018, **39**, 2029–2038.
41 C. Zhang, G. Sun, S. Senapati and H.-C. Chang, *Lab Chip*, 2019, **19**, 3853–3861.
42 J. Fu, J. Gao, R. Pi and P. Liu, *Cytotechnology*, 2005, **49**, 109–116.
43 S. Senapati, Z. Slouka, S. S. Shah, S. K. Behura, Z. Shi, M. S. Stack, D. W. Severson and H.-C. Chang, *Biosens. Bioelectron.*, 2014, **60**, 92–100.
44 L. Sala, B. J. van Meer, L. G. J. Tertoolen, J. Bakkers, M. Bellin, R. P. Davis, C. Denning, M. A. E. Dieben, T. Eschenhagen, E. Giacomelli, C. Grandela, A. Hansen, E. R. Holman, M. R. M. Jongbloed, S. M. Kamel, C. D. Koopman, Q. Lachaud, I. Mannhardt, M. P. H. Mol, D. Mosqueira, V. V. Orlova, R. Passier, M. C. Ribeiro, U. Saleem, G. L. Smith, F. L. Burton and C. L. Mummery, *Circ. Res.*, 2018, **122**, e5–e16.
45 A. Golberg and B. Rubinsky, *Technol. Cancer Res. Treat.*, 2010, **9**, 423–430.
46 T. Hayakawa, T. Kunihiro, T. Ando, S. Kobayashi, E. Matsui, H. Yada, Y. Kanda, J. Kurokawa and T. Furukawa, *J. Mol. Cell. Cardiol.*, 2014, **77**, 178–191.
47 D. Lastochkin, R. Zhou, P. Wang, Y. Ben and H.-C. Chang, *J. Appl. Phys.*, 2004, **96**, 1730–1733.
48 O. Scheel, S. Frech, B. Amuzescu, J. Eisfeld, K.-H. Lin and T. Knott, *Assay Drug Dev. Technol.*, 2014, **12**, 457–469.
49 M. Bébarová, *Gen. Physiol. Biophys.*, 2012, **31**, 131–140.
50 R. A. Bouchard, R. B. Clark and W. R. Giles, *Circ. Res.*, 1995, **76**, 790–801.
51 F. Brette, G. Luxan, C. Cros, H. Dixey, C. Wilson and H. A. Shiels, *Biochem. Biophys. Res. Commun.*, 2008, **374**, 143–146.
52 B. M. Heath and D. A. Terrar, *J. Physiol.*, 2000, **522**, 391–402.
53 O. N. Osipenko, A. Mark Evans and A. M. Gurney, *Br. J. Pharmacol.*, 1997, **120**, 1461–1470.
54 F. Hua, D. C. Johns and R. F. Gilmour, *Am. J. Physiol.*, 2004, **286**, H2342–H2351.
55 X. Li, L. Shen, Z. Fang, X. Zou, Y. He, F. Zhang and C. Zhang, *Sci. Rep.*, 2017, **7**, 1–14.
56 H. Y. Zhongju, L. Zongming and I. S. Cohen, *Pflugers Arch.*, 2004, **447**, 392–400.
57 M. Biel, A. Schneider and C. Wahl, *Trends Cardiovasc. Med.*, 2002, **12**, 206–213.
58 X. Yu, X. Chen, P. Zhou, L. Yao, T. Liu, B. Zhang, Y. Li, H. Zheng, L. Zheng, C. X. Zhang, I. Bruce, J. Ge, S. Wang, Z. Hu, H. Yu, Z. Zhou, X. Yu, C. X-w, P. Zhou, L. Yao, T. Liu, B. Zhang, Y. Li, Z. L-h, Z. Cx, I. Bruce, G. J-b, W. S-q and H. Z-a, *Am. J. Physiol.*, 2007, **292**, 1147–1155.
59 F. Cerignoli, D. Charlot, R. Whittaker, R. Ingermanson, P. Gehalot, A. Savchenko, D. J. Gallacher, R. Towart, J. H. Price, P. M. McDonough and M. Mercola, *J. Pharmacol. Toxicol. Methods*, 2012, **66**, 246–256.
60 Y. Chang, C. N. Broyles, F. A. Brook, M. J. Davies, C. W. Turtle, T. Nagai and M. J. Daniels, *PLoS One*, 2017, **12**, e0174181.
61 A. Chen, E. Lee, R. Tu, K. Santiago, A. Grosberg, C. Fowlkes and M. Khine, *Biomaterials*, 2014, **35**, 675–6839.
62 A. Alassaf, G. Tansik, V. Mayo, L. Wubker, D. Carbonero and A. Agarwal, *Analyst*, 2020, **145**, 139–149.
63 M. L. McCain, A. Agarwal, H. W. Nesmith, A. P. Nesmith and K. K. Parker, *Biomaterials*, 2014, **35**, 5462–5471.
64 S. P. Sheehy, A. Grosberg, P. Qin, D. J. Behm, J. P. Ferrier, M. A. Eagleson, A. P. Nesmith, D. Krull, J. G. Falls, P. H. Campbell, M. L. McCain, R. N. Willette, E. Hu and K. K. Parker, *Exp. Biol. Med.*, 2017, **242**, 1643–1656.

65 A. Korolj, E. Y. Wang, R. A. Civitarese and M. Radisic, *Clin. Sci.*, 2017, **131**, 1393–1404.
66 B. Liau, N. Christoforou, K. W. Leong and N. Bursac, *Biomaterials*, 2011, **32**, 9180–9187.
67 A. P. Petersen, D. M. Lyra-Leite, N. R. Ariyasinghe, N. Cho, C. M. Goodwin, J. Y. Kim and M. L. McCain, *Cell. Mol. Bioeng.*, 2018, **11**, 337–352.
68 D. M. Lyra-Leite, A. M. Andres, A. P. Petersen, N. R. Ariyasinghe, N. Cho, J. A. Lee, R. A. Gottlieb and M. L. McCain, *Am. J. Physiol.*, 2017, **313**, H757–H767.
69 R. R. Besser, M. Ishahak, V. Mayo, D. Carbonero, I. Claure and A. Agarwal, *Theranostics*, 2018, **8**, 124–140.
70 U. I. Can, N. Nagarajan, D. C. Vural and P. Zorlutuna, *Adv. Biosyst.*, 2017, **1**, 1600035.
71 A. C. Zeigler, W. J. Richardson, J. W. Holmes and J. J. Saucerman, *J. Mol. Cell. Cardiol.*, 2016, **94**, 72–81.
72 K. Fountoulaki and N. Dagres, *Card. Fail. Rev.*, 2015, **1**, 64.
73 J. Zhang, R. Tao, K. F. Campbell, J. L. Carvalho, E. C. Ruiz, G. C. Kim, E. G. Schmuck, A. N. Raval, A. M. da Rocha, T. J. Herron, J. Jalife, J. A. Thomson and T. J. Kamp, *Nat. Commun.*, 2019, **10**, 1–15.
74 K. Ronaldson-Bouchard, S. P. Ma, K. Yeager, T. Chen, L. Song, D. Sirabella, K. Morikawa, D. Teles, M. Yazawa and G. Vunjak-Novakovic, *Nature*, 2018, **556**, 239–243.
75 F. Weinberger, I. Mannhardt and T. Eschenhagen, *Circ. Res.*, 2017, **120**, 1487–1500.
76 X. Yang, L. Pabon and C. E. Murry, *Circ. Res.*, 2014, **114**, 511–523.
77 S. Kadota and Y. Shiba, *Curr. Cardiol. Rep.*, 2019, **21**, 73.
78 Y. Jiang, P. Park, S.-M. Hong and K. Ban, *Mol. Cells*, 2018, **41**, 613–621.
79 G. Buzsáki, C. A. Anastassiou and C. Koch, *Nat. Rev. Neurosci.*, 2012, **13**, 407–420.
80 K.-S. Han, C. Guo, C. H. Chen, L. Witter, T. Osorno and W. G. Regehr, *Neuron*, 2018, **100**, 564–578.